Geochimica et Cosmochimica Acta Vol. 54, pp. 2743–2758
Copyright © 1990 Pergamon Press plc. Printed in U.S.A.
0016-7037/90/$3.00 + .00

A poorly crystallized oxyhydroxysulfate of iron formed by bacterial oxidation of Fe(II) in acid mine waters

J. M. BIGHAM,[1,*] U. SCHWERTMANN,[2] L. CARLSON,[3] and E. MURAD[2]

[1]Department of Agronomy, 2021 Coffey Road, The Ohio State University, Columbus, Ohio 43210, USA
[2]Lehrstuhl für Bodenkunde, Technische Universität München, 8050 Freising-Weihenstephan, Germany
[3]Department of Geology, University of Helsinki, PO Box 115, SF-00171 Helsinki, Finland

(*Received December* 7, 1989; *accepted in revised form July* 25, 1990)

Abstract—A poorly crystallized oxyhydroxysulfate of Fe has been identified as the primary component of ochreous precipitates from sulfate-rich mine waters having pH values in the range of 2.5 to 4.0. The compound is characterized by rapid dissolution in acid (pH 3.0) ammonium oxalate, an Fe/S mole ratio ranging from 5 to 8, a high specific surface area (175–225 m^2/g), a yellowish brown (9.0–10.0YR) color, a fibrous morphology, and a broad, 8-line X-ray diffraction profile. Analyses of synthetic analogs prepared by hydrolysis of 0.02 M $FeCl_3$ solutions containing up to 2000 $\mu g/mL$ SO_4 show the material to have a tunnel structure akin to that of akaganéite (β-FeOOH). Sulfate occurs both as a bridging element between Fe atoms lining adjacent walls of the tunnels and as a specifically adsorbed surface component. Extraction of the tunnel SO_4 destabilizes the structure and causes the compound to transform to goethite (α-FeOOH) under ambient conditions. Mössbauer spectra taken at 4.2 K yield hyperfine fields lower than those of even the most poorly crystallized iron oxides, indicating that SO_4 inhibits magnetic ordering. A tetragonal unit cell with a_0 = 1.065 and c_0 = 0.604 nm is proposed to describe the structure. The corresponding unit cell formula is $Fe_{16}O_{16}(OH)_{12}(SO_4)_2$ but may range to $Fe_{16}O_{16}(OH)_{10}(SO_4)_3$ depending upon the degree of saturation of the tunnel and surface sites with SO_4. Because of its abundance and high surface reactivity, this compound should play an important role in regulating the solubilities of both major and trace elements in surface waters impacted by acid mine drainage.

INTRODUCTION

THE ATMOSPHERIC OXIDATION of iron sulfides occurring in ore and coal deposits, and the subsequent release of H_2SO_4 and Fe to leaching waters, is a well-known phenomenon. The process has been commercially exploited for the concentration of trace metals through solution mining of ores and tailings; however, it has also become a scourge in some areas due to the uncontrolled release of acid effluents into streams and lakes from abandoned mines and spoils. Sulfide dissolution under Earth-surface conditions is a complex biogeochemical process involving numerous hydrolysis and redox reactions as well as microbial catalysis (NORDSTROM, 1982). While mechanistic details of many subreactions are lacking, the general process has been described as follows (KLEINMANN et al., 1981):

$$FeS_2 + 3.5O_2 + H_2O \rightarrow Fe^{2+} + 2H^+ + 2SO_4^{2-}, \quad (1)$$

$$Fe^{2+} + 0.25O_2 + H^+ \rightarrow Fe^{3+} + 0.5H_2O, \quad (2)$$

$$FeS_2 + 14Fe^{3+} + 8H_2O \rightarrow 15Fe^{2+} + 2SO_4^{2-} + 16H^+, \quad (3)$$

$$Fe^{2+} + 2.5H_2O + 0.25O_2 \rightarrow Fe(OH)_{3(s)} + 2H^+. \quad (4)$$

The most emphasis to date has been placed on understanding the initial abiotic/biotic oxidation mechanism (reaction 1), the subsequent microbial oxidation of Fe^{2+} under acid (pH < 3.0) conditions (reaction 2), and the accelerated oxidation of the metal sulfide by dissolved Fe^{3+} (reaction 3). In contrast, the final off-site oxidation and hydrolysis of Fe (reaction 4) has been little studied, even though the labile character of the sediment produced by this reaction (MCKNIGHT et al., 1988) and its scavenging potential for some metal species (CHAPMAN et al., 1983; FILIPEK et al., 1987; KARLSSON et al., 1987) have recently been documented.

Most technical sources refer to the precipitate produced in streams and lakes receiving acid mine drainage as simply "amorphous ferric hydroxide" (e.g., STUMM and MORGAN, 1981). A few more detailed studies have suggested the presence of ferrihydrite (FERRIS et al., 1989), feroxyhite (CROSBY et al., 1983), and/or jarosite (FILIPEK et al., 1987), even though water analyses and geochemical calculations frequently indicate equilibrium with a sulfate-bearing phase having a solubility (at ≃ pH 3) higher than those of jarosite or the common iron oxides (CHAPMAN et al., 1983; FILIPEK et al., 1987; SULLIVAN et al., 1988; KARATHANASIS et al., 1988). BRADY et al. (1986) recently identified such a compound but were unable to fully characterize the mineral or define its structure due to poor crystallinity and the presence of associated goethite (α-FeOOH). In this paper we present results from both synthetic and natural specimens to show that a sulfate-rich oxyhydroxide with a tunnel structure akin to that of akaganéite (β-FeOOH) is the so-called "amorphous iron hydroxide" associated with many mine drainage waters.

MATERIALS AND METHODS

Natural Specimens

The specimen set includes five sediment samples collected from mine effluents in the eastern Ohio coalfield and from drainage exiting an abandoned copper-arsenic mine in Finland. These samples were selected on the basis of mineralogical purity from a larger set of 43

* To whom correspondence should be addressed.

specimens acquired from several locations in the United States, Europe, and Australia. Most of these samples contained the mineral in question, and their full mineralogical variability will be described elsewhere. Additional site details for those materials included in this paper are provided in Table 1. All samples were obtained as fluid bottom sediments that were subsequently gravity sedimented in water to partially exclude coarse-grained mineral particles of detrital origin and to remove excess salts. Fine (<6 μm) fractions were either freeze dried or dried at 40°C after centrifuging to remove excess water. Separate water samples were collected from the acidic effluents and were transported under ice to the laboratory where they were subsequently analyzed for Cl^-, SO_4^{2-}, total dissolved Fe, Fe^{2+}, and a variety of other dissolved metals; pH was measured both in the field and laboratory. Analytical details for the Ohio water samples are provided by WINLAND (1989).

Preparation of Laboratory Specimens

Sulfate-bearing specimens analogous to those occurring in the field were successfully prepared using both abiotic and biotic approaches. Abiotic samples were synthesized by hydrolyzing a series of 0.02 M $FeCl_3$ solutions containing 0, 62, 125, 250, 500, 750, 1000, 1500, and 2000 μg/mL SO_4^{2-} (as Na_2SO_4) for 12 min at 60°C. After cooling to room temperature, the suspensions were dialyzed for 30 days against deionized water using cellulose membranes with an average pore radius permeability of 2.4 nm. Initial pH values ranged from 2.09 (0 μg/mL SO_4^{2-}) to 2.25 (2000 μg/mL SO_4^{2-}). Following dialysis, all precipitates were freeze dried.

Additional specimens were synthesized by bacterial oxidation of $FeSO_4 \cdot 7H_2O$ solutions at pH 2.0 to 3.0 using a strain of *Thiobacillus ferrooxidans* (acquired from Deutsche Sammlung von Mikroorganismen und Zellkulturen GmbH; DSM-Nr.: 583) and a batch fermentation system (B. Braun, model Biostat M) with a 1 L reaction vessel instrumented to provide constant temperature, controlled stirring, and continuous readout of pH and redox potential. The sample described in this paper was prepared by adding 200 mL of feed solution [0.2% $(NH_4)_2SO_4$, 0.01% KCl, 0.025% $MgSO_4$, 0.025% K_2SO_4, 0.001% $Ca(NO_3)_2$, 4.0% $FeSO_4$, pH 1.4 with H_2SO_4] containing acclimated bacterial cells to 800 mL of a 4.0% $FeSO_4$ solution to yield a system with an initial pH of 2.9 and redox potential of 270 mV. Temperature and stirring rate were maintained constant at 24°C and 500 rpm, respectively. Within 10 days, the pH of the system decreased to 1.4, the redox potential stabilized at 825 mV, and NH_4-jarosite precipitated in the reaction vessel. This material was separated by centrifugation, and the brown colloid remaining in suspension was flocculated by slow titration to pH 4.0 with 0.1 M NaOH. The precipitate thus collected (identified as Z510b) was water washed by centrifugation and freeze dried. A separate but similar biological specimen (Z500a) was utilized for Mössbauer spectroscopic studies and has been described elsewhere (MURAD, 1988).

Analytical Methods

Total sulfur (S_t) and carbon (C_t) were obtained by a combustion procedure using either a Leco Model 521 or a Leybold-Heraeus Series 302 induction furnace. With the former, SO_2 evolved at 1000°C was collected in a starch solution and measured using a semiautomatic titrator with KIO_3 as the titrant. With the latter, both SO_2 and CO_2 were measured directly with an infrared analyzer after combustion in an O_2 atmosphere at 1000°C. Total oxide Fe (Fe_t) in the samples was determined after cold dissolution with 5M HCl. Acid insoluble residues from the extraction were washed, dried, and weighed. Oxalate-extractable Fe (Fe_o) was determined according to the method of SCHWERTMANN (1964) using both 15 and 120 min extraction times in the absence of light. Iron in all extracts was measured by atomic absorption spectroscopy. Total Cl (Cl_t) was measured colorimetrically after dissolution of 40 mg of sample in 4 mL of 60% $HClO_4$ over an open flame. Following dissolution, the solution was brought to 20 mL volume and a 5 mL aliquot was mixed with 4 mL of 0.25% HNO_3 and 4 mL of a color reagent containing $Hg(SCN)_2$, methanol, and $Fe(NO_3)_3$. This solution was diluted to 25 mL and the absorbance at 490 nm was measured after 10 min (FARZANEH and TROLL, 1978). Total As was determined either by neutron activation analysis at the University of Wisconsin Nuclear Reactor Laboratory in Madison, Wisconsin, USA, or after cold dissolution of the samples with 12.5 M HCl. In the latter procedure, As was reduced to the trivalent state by treatment with KI and $SnCl_2$. Arsenic was subsequently liberated in the presence of elemental Zn and absorbed in a solution of silver diethyldithiocarbamate in chloroform-quinoline. The reddish-brown As complex was then quantified colorimetrically at 545 nm (MARSHALL, 1978).

Dissolution-time curves were constructed by a batch procedure in which duplicate, 10 mg samples were continuously shaken in 10 mL of 0.1M HCl for predefined time periods ranging from 0.25 to 24 h. After quenching of the reaction through filtration, dissolved Fe was determined by atomic absorption spectroscopy and SO_4 by ion chromatography.

X-ray diffraction (XRD) analyses of backfill powder mounts were conducted using CoKα radiation with a Philips PW1070 goniometer equipped with a diffracted-beam monochromator and a 1° divergence slit. All specimens were step scanned from 10 to 80°2θ in increments of 0.05°2θ and with 20 sec counting time. The digitized scans were then fitted with the FIT curve program of JANIK and RAUPACH (1977) as modified by H. Stanjek (unpubl. data). Unit-cell edge lengths were subsequently calculated with the program GITTER (W. Hummel, unpubl. data) using six tan θ weighted reflections.

Mössbauer spectra (MURAD, 1988; MURAD et al., 1988) were taken on samples mixed with two parts sugar using a ^{57}Co/Rh source. The samples were placed in plastic sample holders to produce absorbers with Fe concentrations of about 9–16 mg/cm^2. Spectra were taken at room temperature, between 90 and 70 K, and at 4.2 K while cooling both source and absorber in a bath cryostat over different velocity ranges between ±2 and ±10 mm/sec until $1.1 \cdot 10^6$ to $9.4 \cdot 10^6$ counts per channel had been collected. Spectra of selected samples were also taken under applied magnetic fields up to 9 T. The transmitted radiation was recorded with a proportional counter and stored in a multichannel analyzer. The mirror halves of the spectra were folded and Lorentzian line fits carried out by a computer procedure constraining corresponding lines of every doublet and sextet to have equal widths and intensities. Isomer shifts are given relative to the centroid of the room-temperature spectrum of metallic Fe.

Infrared (IR) absorption spectra were recorded with a Beckman IR-4250 spectrometer from 200 to 4000 cm^{-1} using KBr pellets (0.3% sample) and a scan speed of 150 cm^{-1}/min. Specific surface areas were determined by ethylene glycol monoethyl ether (EGME) adsorption (CARTER et al., 1965). The precision of the EGME method is about 5% based on calibrations with a ZnO powder having a BET surface area of 48 m^2/g. Colors of both the synthetic and natural samples were obtained from powdered specimens using a double-beam Perkin Elmer, Lambda-3 spectrophotometer equipped with a reflectance integrating sphere attachment; the reflectance measurements were converted to Munsell notations according to the procedure described by TORRENT and SCHWERTMANN (1987). Simultaneous differential thermal and thermogravimetric analyses (DTA, TGA) were performed with a Linseis instrument operated at a heating rate of 10°C/min in air with 40–50 mg of dry (over P_2O_5) sample and hematite as an inert reference material. Weight losses after static heating to 100 and 800°C for 12–18 h were also determined for the natural and selected synthetic specimens. Finally, transmission electron micrographs (TEM) were obtained with a Zeiss EM 10 A/B electron microscope.

Table 1. Location of sample sites

Sample	Location	Lat./Long.
Bt-4	Belmont Co., Ohio, USA	40° 07′N 80° 45′W
La-1	Lawrence Co., Ohio, USA	38° 48′N 82° 37′W
Nb-1	Noble Co., Ohio, USA	39° 43′N 81° 27′W
Y1	Ylöjärvi District, Finland	61° 36′N 23° 30′E
Y3b	Ylöjärvi District, Finland	61° 36′N 23° 30′E

Table 2. Water chemistry

Sample	pH	SO_4^{2-}	Cl^-	Fe^{2+}	Fe_{total}	Mn^{2+}	Ca^{2+}	Mg^{2+}	K^+	Na^+
					μg/mL					
Bt-4	3.2	1257	28	110	127	1	167	32	2	49
La-1	3.1	1242	44	69	94	1	220	34	5	28
Nb-1	3.0	4343	39	19	81	59	576	481	11	11
Y1	4.9	168	<1	2	2	<1	15	2	4	2
Y3b	3.1	872	7	66	74	8	123	36	12	31

RESULTS AND DISCUSSION

Chemical Composition of Source Waters and Mineral Samples

Waters collected with the sediments had pH values ranging from 3.0 to 4.9 (Table 2) and, with one exception, were within the range of 2.0–3.5 normally reported for acid mine drainage (FENCHEL and BLACKBURN, 1979). Sulfate was the dominant anion in each system, even though absolute concentrations varied by a factor of 25 from 168 to 4343 μg/mL. In all cases, some Fe^{2+} remained in solution with variable quantities of associated alkali and alkaline earth cations. Detailed analyses of both major and trace constituents in the Ohio water samples are given by WINLAND (1989).

Secondary iron precipitates comprising the bulk of each sediment sample were readily dissolved in the course of a 10–20 min extraction with 5 M HCl. The gray, acid-insoluble residues consisted primarily of quartz, feldspars, and phyllosilicates and represented 1 to 12.5% of the original samples (Table 3). When adjusted for the weight of these detrital minerals, the Fe and SO_4 contents of the ochreous precipitates average 43 and 13%, respectively, and are comparable to those of the biotic (Z510b) and abiotic laboratory preparations formed at high sulfate concentrations. Samples in the latter series appear to approach a maximum of approximately 12% SO_4 (Table 4). Oxide summations including Cl_t and with corrections for the detrital mineral fractions range between 99 and 102% and indicate complete analysis of the acid soluble materials (Table 5). Fe/S mole ratios in the mine precipitates range from 4.7 to 8.3 and, in general, compare favorably with the ratio of 5.0 obtained by JACOBSEN (1976) and LAZAROFF et al. (1985) from similar sediments. In contrast, stoichiometric jarosite $[KFe_3(SO_4)_2(OH)_6]$ contains 38.4% SO_4 and yields an Fe/S mole ratio of 1.5.

Oxalate Solubility

Acid ammonium oxalate at pH 3.0 has been widely used as a selective extractant of poorly crystallized Fe-oxides from soils and sediments. The HCl-soluble fraction of the mine drainage samples is almost completely soluble in oxalate; hence, ratios of oxalate-extractable to total oxide Fe (Fe_{o120}/Fe_t) approach unity (Table 3) and are indicative of a material having only short-range structural order (SCHWERTMANN and FISCHER, 1973; CARLSON and SCHWERTMANN, 1981). Increasing values of Fe_{o120}/Fe_t in the synthetic specimens are associated with increasing SO_4 and decreasing Cl contents (Table 4). BRADY et al. (1986) noted similar trends in Cl-free specimens prepared from $Fe(NO_3)_3$; therefore, it appears that SO_4 may have a positive influence on reactivity of the solid phase toward oxalate.

The dissolution reaction in oxalate is complete for most of the sediment samples within 15 min as indicated by ratios of Fe_{o15}/Fe_{o120} near unity (Table 3). Comparable rates were achieved with the synthetic specimens only when SO_4 contents exceeded 11% (Table 4). Natural sample Y1, with Fe_{o15}/Fe_{o120} equal to 0.85, likewise contains less than 11% SO_4.

Surface Area, Color, and Particle Morphology

A marked change in the physical characteristics of the synthetic B-series samples is also associated with SO_4 contents in the range of 11 to 12% (Table 4). Specimens containing <11.5% SO_4 consist of rod-shaped particles that are reddish brown to dark reddish brown in color and densely aggregated when dried. Because of this strong tendency to aggregate, the measured surface areas are probably conservative estimates since the EGME molecules might not have access to all particle surfaces. This is particularly true for sample B-0S which was a stable sol before drying. Electron microscopy (Fig. 1a) shows this sample to consist of particles that are only 3–6 nm in diameter, yet the surface area is one of the lowest measured at 250 m^2/g. Mine sediment sample Y1, with 8.5% SO_4, is also composed of rod-shaped particles (Fig. 1e) and

Table 3. Properties[1] of natural samples

Sample	Specific Surface (m^2/g)	$SO_{4(t)}$	$Fe_{o(15)}$	$Fe_{o(120)}$	Fe_t	C_t	Cl_t	$Fe_{o(15)}/Fe_{o(120)}$	$Fe_{o(120)}/Fe_t$	A.I.R.	Color	As_t
		%								%		%
Bt-4	225	14.1	38.8	39.4	39.4	1.0	0.4	0.98	1.00	10.5	9.3YR 6.2/7.5	0.4
La-1	196	12.1	35.6	37.1	37.7	2.4	0.9	0.96	0.98	12.1	0.2Y 6.7/7.0	Ndt
Nb-1	199	13.9	40.5	41.1	40.7	0.7	0.2	0.97	1.00	10.0	9.7YR 6.8/7.4	<0.1
Y1	229	8.5	32.3	37.9	41.1	2.8	1.6	0.85	0.92	4.5	9.0YR 6.2/8.0	0.7
Y3b	175	10.7	41.3	41.3	41.8	3.1	1.2	1.00	0.99	1.1	n.d.	1.2

[1] $SO_{4(t)}$ = total sulfate; $Fe_{o(15)}$ = Fe extractable with oxalate in 15 min; $Fe_{o(120)}$ = Fe extractable with oxalate in 120 min; Fe_t = Fe extractable with 5M HCl; A.I.R. = 5M HCl insoluble residue; C_t = total carbon; Cl_t = total chloride; As_t = total arsenic. All values except color derived from duplicate or triplicate analyses. N.d. = not determined. Ndt = not detected.

Table 4. Properties[1] of synthetic samples

Sample	Specific Surface (m^2/g)	$SO_{4(t)}$	$Fe_{o(18)}$	$Fe_{o(120)}$	Fe_t	$Fe_{o(18)}/Fe_{o(120)}$	$Fe_{o(120)}/Fe_t$	Color	Cl
		%							%
B-0S	249	0.1	6.8	24.2	56.7	0.28	0.43	4.9YR 3.6/5.3	1.5
B-62S	316	4.9	18.1	37.8	51.2	0.48	0.74	5.7YR 4.1/6.0	0.8
B-125S	307	6.8	30.2	45.7	49.9	0.66	0.92	6.1YR 4.2/6.3	0.6
B-250S	337	9.6	38.9	45.2	48.2	0.86	0.94	5.4YR 3.1/4.8	0.3
B-500S	347	11.4	43.3	44.8	46.5	0.97	0.96	6.2YR 3.4/5.6	0.2
B-750S	311	11.7	43.4	44.9	47.6	0.97	0.94	7.6YR 4.7/7.1	0.1
B-1000S	319	11.7	44.7	45.1	45.8	0.99	0.98	9.2YR 6.4/8.1	0.1
B-1500S	262	12.0	45.1	45.4	46.3	0.99	0.98	9.0YR 6.2/9.1	0.1
B-2000S	240	12.3	45.4	45.9	45.9	0.99	1.00	9.1YR 6.2/9.1	0.1
Z510b (biotic)	120	15.5	42.0	43.2	43.2	0.97	1.00	n.d.	<0.1

[1] see Table 2 for definition of terms.

has the highest specific surface area of the natural materials (Table 3).

As SO_4 contents approach 11.5% in the B-series samples, the particles become more acicular (Fig. 1b) and eventually coalesce (Fig. 1c) to form rounded aggregates that are 200 to 500 nm in diameter with electron-dense interiors and "grassy" surfaces (Fig. 1d). Although the aggregates have the appearance of single crystals, selected area electron diffraction (data not given) has shown them to be polycrystalline. These samples are distinctly yellow in color (Table 4) and are voluminous both in suspension and upon drying. The natural precipitates (except specimen Y1) exhibit similar colors, surface areas, and morphologies and are also voluminous in character (Table 3, Fig. 1e).

Using scanning electron microscopy, LAZAROFF et al. (1985) described "amorphous" bacterial precipitates produced in similar fashion to sample Z510b and also noted a filamentous morphology that they termed fibroporous. This filamentous morphology appears typical of the ochreous precipitates from many acid sulfate environments (BRADY et al., 1986; LAZAROFF, et al., 1985; FERRIS, et al., 1989) and contrasts sharply with those of jarosite and ferrihydrite. The former is usually composed of pseudocubic crystals (Fig. 1e), whereas the latter is comprised of highly aggregated, spherical particles with diameters in the order of 2 to 6 nm (TOWE and BRADLEY, 1967).

X-ray Diffraction Data

With the exception of sample Y1, diffractometer tracings from the mine sediments (Fig. 2) consist of eight broad diffraction bands with superimposed sharp peaks due primarily to detrital quartz and silicate minerals. Minor to trace amounts of goethite (Gt) are present in four of the five specimens, and sample Nb-1 (not shown) also contains trace amounts of jarosite. Sample Y3b is essentially free from im-

Table 5. Total chemical analyses[1]

Sample	Fe_2O_3	As_2O_3	SO_3	CO_2	$H_2O_{(100)}$[2]	$H_2O_{(800)}$[3]	Cl	Σ	Fe/S
	%								
Bt-4	63.0	0.6	13.1	4.2	8.8	11.3	0.4	101.4	4.7
La-1	61.3	-	11.5	9.9	8.8	9.3	1.0	101.8	5.4
Nb-1	64.7	-	12.9	2.8	7.4	12.9	0.2	100.9	5.0
Y1	61.5	1.2	7.4	10.6	9.1	8.1	1.7	99.6	8.3
Y3b	60.4	1.9	9.0	11.5	10.4	6.8	1.2	101.2	6.7
Z510b	61.8		12.9		9.8	14.1	-	98.6	4.8
B-2000S	65.6		10.2		8.9	14.9	0.1	99.7	6.4

[1] Data corrected for detrital mineral fraction.
[2] $H_2O_{(100)}$ = weight loss after drying at 100°C for 12 - 18 hr;
[3] $H_2O_{(800)}$ = weight loss after drying at 800°C for 12 - 18 hr less [$H_2O_{(100)}$ + SO_3 + CO_2 evolved at 1000°C] (see discussion of TGA results).

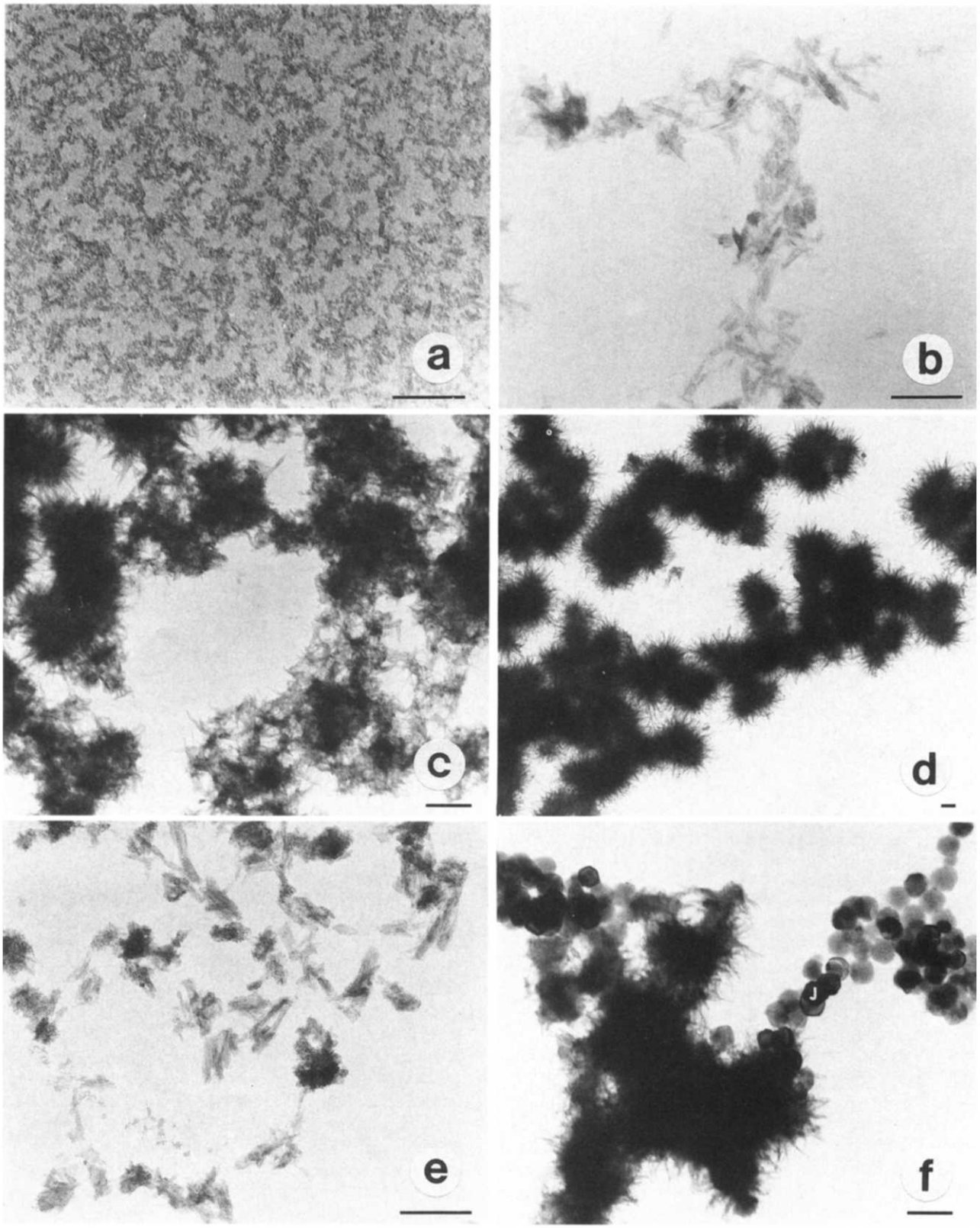

FIG. 1. Transmission electron micrographs of synthetic samples (a) B-0S, (b) B-750S, (c) B-1000S, (d) B-2000S, and natural precipitates (e) Y1 and (f) Nb-1 with jarosite crystals identified as "J." Bar represents 0.1 μm.

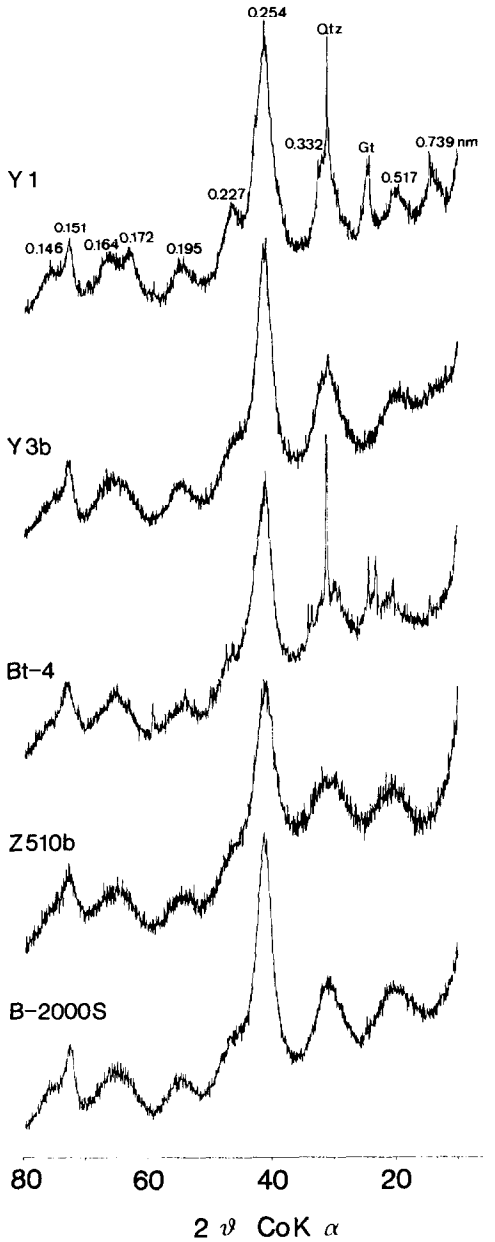

FIG. 2. X-ray powder diffraction patterns from representative sediment samples and the high SO_4 synthetic specimens (Z510b and B-2000S).

purities. Peak position and line width data for the 8-line diffraction profiles of specimens Bt-4, La-1, Nb-1, and Y3b are in agreement with results obtained from synthetic specimens Z510b (biotic) and B-2000S (abiotic) (Fig. 2, Table 6). In all cases, the broad but consistent character of the diffraction maxima indicates a material that is poorly crystallized but certainly not X-ray amorphous. Structural relationships between these samples and specimen Y1, which yields two additional XRD lines at 0.739 and 0.172 nm (Fig. 2), can be clarified by considering data from the complete series of synthetic materials (Fig. 3).

In this series, the material prepared by hydrolysis of 0.02 M $FeCl_3$ solution without added SO_4 (sample B-0S) is a pure but poorly crystallized akaganéite containing 1.5% Cl and displaying all the diagnostic X-ray lines for β-FeOOH (MURAD, 1979) (Table 4, Fig. 3). Well-crystallized specimens of synthetic akaganéite usually contain 3–9% Cl (KELLER, 1970; ISHIKAWA and INOUYE, 1975; ELLIS et al., 1976; MURAD, 1979; CHILDS et al., 1980; PATERSON et al., 1982), and the (110) and (310) reflections at 0.75 and 0.33 nm, respectively, comprise the most intense diffraction lines. In sample B-0S both of these peaks are reduced in intensity relative to the (211) reflection at 0.254 nm and all peaks are noticeably broadened, suggesting a possible relationship between Cl content and crystallinity. To test this possibility, a subsample of B-0S was equilibrated for 90 days in a 0.05 M solution of $AgNO_3$ to extract structural Cl. The $AgNO_3$ effectively lowered the Cl content from 1.5 to 0.9% through formation of AgCl with no apparent effect on X-ray line intensities or breadths. ISHIKAWA and INOUYE (1975) likewise reported no change in the X-ray diffraction profile of a synthetic akaganéite when its Cl content was reduced from 6.3 to 2.7 wt% by exhaustive washing.

Addition of SO_4 to the initial hydrolysis solutions in amounts ranging from 62 to 2000 μg/mL caused further broadening of all peaks relative to sample B-0S (Fig. 3). Progressive reductions in the intensities of the (110) and (310) peaks at low SO_4 levels (62–250 μg/mL) are especially evident and are consistent with the suggestion of TOWE (1981) that these spacings may be particularly sensitive to decreasing particle size and/or crystallinity. At higher SO_4 concentrations (750–2000 μg/mL), the (110) line is completely suppressed. When I*WHH (product of intensity and full width at half height with correction for background) of the (110) peak is plotted as a function of total SO_4 (Table 4), a linear relationship is observed in the B-series samples, suggesting that the reduced intensity of the (110) line is directly related to SO_4 content (Fig. 4). Over the same concentration range, Cl is essentially eliminated from the synthetic samples, indicating a strong competitive effect from SO_4 that is presumably related to its higher charge and its ability to form inner sphere complexes with structural Fe.

When the regression line in Fig. 4 is extrapolated to I*WHH(110) = 0, the corresponding SO_4 content is 10.7%. All natural specimens not showing a (110) diffraction line contain ≥10.7% SO_4 and variable (0.2–1.3%) amounts of Cl. Specimen Y1, with only 8.5% SO_4, contains 1.6% Cl and exhibits not only a weak 0.74 nm reflection but also resolved peaks at 0.172 and 0.164 nm corresponding to the (600) and (521) lines, respectively, of akaganéite (Figs. 2 and 3). As SO_4 contents of the synthetic specimens increase from near 0 to 11.4% (B-0S to B-500S), the (600) peak weakens and is gradually displaced by the (521) to yield a single diffraction band centered at approximately 0.166 nm (Fig. 3, Table 6). In addition, the (200) reflection undergoes an *apparent* shift toward lower spacings, the (301) broadens to form a shoulder on the high angle side of the intense (211) peak, and multiple reflections in the range of 74 to 78°2θ (corresponding to the 611, 710, 550, 112, 202, and 541 lines of akaganéite) coalesce to form a single broad diffraction band. The net result is an 8-line diffraction profile like those of natural specimens Bt-4, La-1, Nb-1, and Y3b. Sample Y1, which is almost identical to synthetic sample B-250S, appears to represent a transitional

Table 6. X-Ray results

hkl (proposed)	hkl (β-FeOOH)	Natural Specimens								Synthetic Specimens			
		Bt-4		La-1		Nb-1		Y3b		Z510b		B-2000S	
		d nm	WHH °2θ	d nm	WHH °2θ	d nm	WHH °2θ	d nm	WHH °2θ	d nm	WHH °2θ	d nm	WHH °2θ
	110												
(200,111)	200	0.483	5.9	0.487	5.7	0.491	4.8	0.521	3.0	0.502	7.0	0.512	6.1
310	310	0.338	7.4	0.341	5.5	0.336	6.3	0.333	3.6	0.334	8.1	0.336	4.4
212	211	0.254	3.3	0.254	3.3	0.255	3.1	0.255	2.9	0.255	4.1	0.255	3.0
302	301	0.233	6.2	0.232	6.4	0.237	6.6	0.232	4.6	0.227	4.7	0.230	5.4
412	411	0.195	3.2	0.195	3.0	0.193	1.6	0.194	3.1	0.195	3.6	0.194	3.9
	600												
522	521	0.165	7.0	0.166	6.7	0.166	5.5	0.166	6.3	0.166	7.6	0.166	6.7
004	002	0.151	3.8	0.151	3.4	0.151	3.4	0.151	1.6	0.151	3.2	0.151	1.6
(204,542)	541	0.143	8.2	0.144	9.3	0.146	8.8	0.146	9.3	0.145	10.1	0.146	9.5
	a_o	1.063±0.004		1.072±0.004		1.063±0.010		1.063±0.005		1.062±0.004		1.066±0.005	
	c_o	0.604±0.001		0.603±0.001		0.604±0.003		0.605±0.001		0.604±0.001		0.605±0.002	

phase and provides a strong link between the natural and synthetic specimens. Although XRD data clearly indicate that the structure of the mine drainage mineral is similar to that of akaganéite, other results yet to be discussed suggest that a modified structure and different line indexing may, in fact, be appropriate.

Thermal Behavior

Thermal decomposition of the mine precipitates produces a low-temperature endotherm between 100 and 300°C followed by an exotherm at 540 to 580°C that immediately gives way to a second endothermic reaction centered at approximately 680°C (Fig. 5). Similar results were achieved by MARGULIS et al. (1975) from a synthetic gel with composition $2Fe_2O_3 \cdot SO_3 \cdot mH_2O$. Samples Y1, Y3b, and La-1 (not shown) exhibit an additional broad exothermic effect between 300 and 460°C that is primarily due to combustion of organic matter.

The initial endothermic reaction is associated with a weight loss of 15 to 20% that probably derives from the vaporization of a monolayer of chemisorbed H_2O (SCHWERTMANN et al., 1985) as well as structural OH/H_2O. XRD analyses of samples taken after quenching of the thermal reaction at 300°C indicate the presence of a disordered variety (or modification) of the mine drainage mineral which yields a broad, asymmetric diffraction band with maximum intensity at 0.254 nm. By 460°C, this material is at least partially converted to poorly crystallized hematite. The extent of hematite transformation appears to be negatively related to the SO_4 content, indicating a possible inhibitory effect on structural reorganization in much the same manner as Si represses the thermal decomposition of ferrihydrite to hematite (CARLSON and SCHWERTMANN, 1981). MACKENZIE (1957) also noted that the thermal alteration of "ferric oxide gels" to hematite was delayed by adsorbed SO_4.

Just prior to onset of the exothermic reaction at 560°C all samples consist of hematite with substantially improved crystallinity, as reflected in XRD peak widths. Products immediately after the reaction include both hematite and $Fe_2(SO_4)_3$, indicating that crystallization of the latter could be responsible for the observed exothermic effect; however, thermal decomposition of a sulfatic, poorly crystallized goethite (data not presented) also yielded $Fe_2(SO_4)_3$ but without a corresponding exotherm. A slight weight loss in the temperature range 600 to 640°C is consistently expressed in DTGA curves (Fig. 5) and suggests that the high-temperature exotherm is largely produced by further expulsion of water during recrystallization of hematite. The final endotherm at 680°C can be attributed to decomposition of $Fe_2(SO_4)_3$ to yield additional hematite and SO_3. Volatilization of the latter produces a weight loss of 6 to 12%.

Infrared Characteristics

LAZAROFF et al. (1982) studied in detail the IR properties of ochreous precipitates produced by bacterial oxidation of acid ferrous sulfate solutions in the laboratory. Major products included a variety of jarosites and a material described as "amorphous ferric hydroxysulfate." Experimental data obtained from the latter substance correspond well with those produced in the present study (Fig. 6, Table 7); however, our interpretations of these results differ significantly.

In their analyses, LAZAROFF et al., (1982) describe a single, broad $\nu_3(SO_4)$ absorption band at 1110–1120 cm^{-1} with a shoulder at 1170 to 1180 cm^{-1} due to "additional sulfate IR activity." Bands at 970 to 980 and at 1045 cm^{-1} were assigned to $\nu_1(SO_4)$ and δ(OH), respectively. The latter assignment was based on residual absorption at 1045 cm^{-1} following *partial* replacement of SO_4 by SeO_4 which exhibits a ν_3 mode at a substantially lower (870 cm^{-1}) frequency. Additional bands at 670–690, 610–620, and 410–460 cm^{-1} were observed but not assigned. Later, LAZAROFF (1983) and LAZAROFF et al. (1985) attributed the 690 cm^{-1} band to the hindered rotation (ν_r) of H_2O.

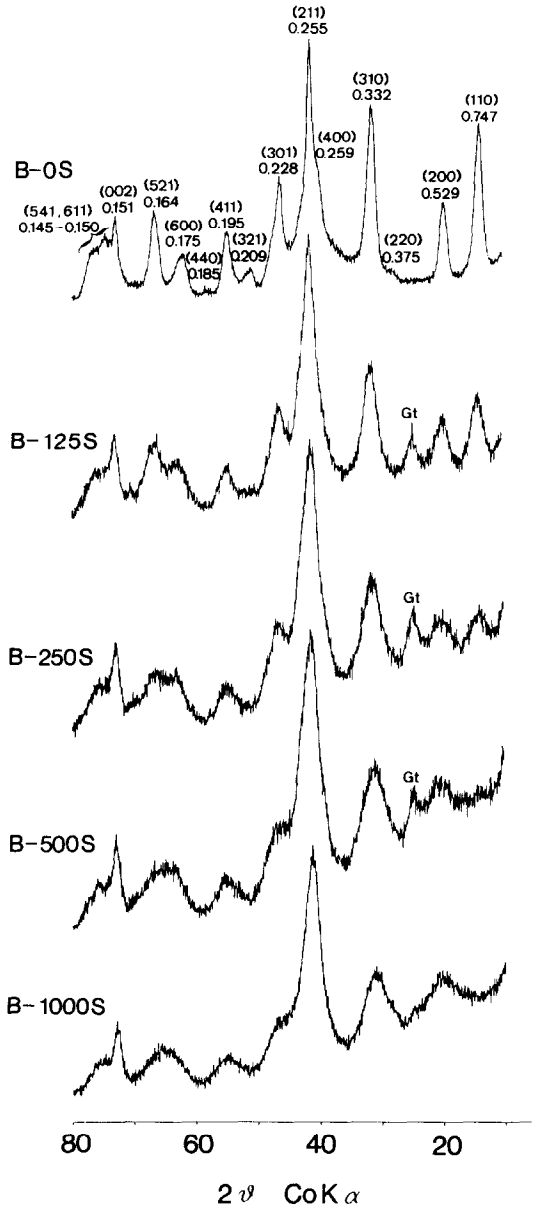

FIG. 3. X-ray powder diffraction patterns from laboratory specimens prepared by hydrolysis of 0.02 M $FeCl_3$ in the presence of 0, 125, 250, 500, and 1000 μg/mL SO_4. Indices for sample B-0S are based on the akaganéite unit cell.

Apparently because of the rather diffuse character of the primary $\nu_3(SO_4)$ feature, LAZAROFF et al. (1982, 1985) assigned T_d symmetry to the SO_4 in their samples. T_d symmetry is typical of the free ion state in which only the ν_3 and ν_4 fundamental bands should be infrared active (HARRISON and BERKEISER, 1982). If the symmetry of SO_4 decreases with coordination, a splitting of the ν_3 fundamental occurs. For a unidentate complex (C_{3v} symmetry) two bands appear as in jarosite (POWERS et al., 1975), and for a bidentate complex (C_{2v} symmetry) three bands should be present. Appearance of the ν_1 mode also indicates low site symmetry for SO_4.

To resolve the question of a contribution from δ(OH) in the 1040–1070 cm^{-1} region a completely selenated analog of synthetic sample B-2000S was prepared (to be described elsewhere) as attempted by LAZAROFF et al. (1982). No absorption was observed in this region when SO_4 was excluded, indicating that the band reported by LAZAROFF et al. (1982) was due to ν_3 absorption from residual SO_4 and not from δ(OH). Thus, the intense band at 1125 cm^{-1} and the associated shoulders at 1170 to 1180 and 1040 to 1070 cm^{-1} must arise from the formation of a bidentate complex between SO_4 and Fe in the mine drainage precipitate. Such complexes may form by replacement of OH groups with SO_4 at the mineral surface through ligand exchange or within the structure during nucleation and subsequent growth of the crystal. The bonds resulting from these two binding sites are probably similar in energy and geometry, and, as a result, may be difficult to distinguish by IR spectroscopy.

For example, PARFITT and SMART (1978) and HARRISON and BERKHEISER (1982) observed a strong splitting of the $\nu_3(SO_4)$ fundamental with adsorption of SO_4 on "amorphous" iron oxide. The published spectra from their samples are similar to those in Fig. 6 over the range of 900 to 1200 cm^{-1} and include a band at 970 cm^{-1} due to $\nu_1(SO_4)$. To further examine the contribution of adsorbed SO_4 in the present study, sample B-0S was subsampled after aging in dialysis but before drying. This material was subsequently equilibrated for 30 days against a solution containing 2000 μg/mL (20.8 μm/mL) SO_4 as employed in the preparation of sample B-2000S. After washing with distilled H_2O and drying, the sulfated subsample of B-0S retained 2.9% SO_4 as compared to 12.2% SO_4 in sample B-2000S (both with a measured surface area of approximately 250 m^2/g). The infrared spectrum from the sulfated specimen (Fig. 6) shows weak but clearly discernable splitting of $\nu_3(SO_4)$ as well as absorbance due to $\nu_1(SO_4)$; however, the intensities of these lines are much weaker than in the mine precipitates. From these results it is apparent that adsorbed SO_4 may be significant, but it cannot account for the full SO_4 content of the mine precipitates.

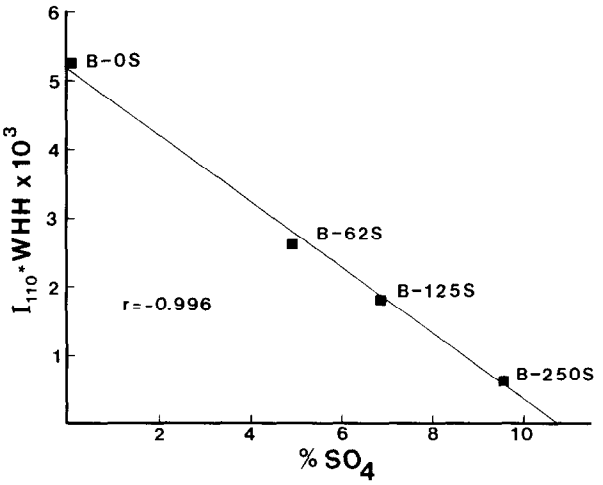

FIG. 4. Relationship between total sulfate content and the product of the intensity and width at half height of the (110) X-ray diffraction peak.

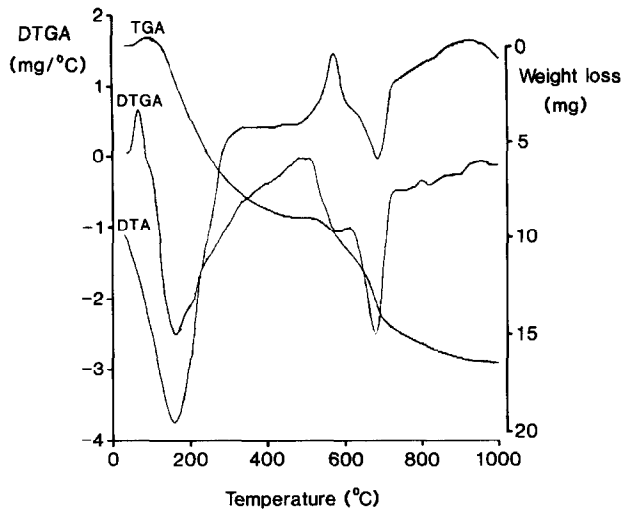

FIG. 5. Differential thermal (DTA), thermogravimetric (TGA), and differential thermogravimetric (DTGA) patterns from sample Bt-4. Total initial sample weight = 57.4 mg.

Because of structural similarities, further clarification of IR results from the mine drainage materials can be expected by analysis of the infrared characteristics of akaganéite. The IR spectrum of a well-crystallized specimen of akaganéite usually includes two bands at 640 and 840 cm^{-1} due to OH deformation [δ(OH)] and two additional bands at 690 and 410–460 cm^{-1}, the latter of which can be attributed to Fe-O stretch (Fig. 6). By comparison, the poorly crystallized β-FeOOH prepared in this study (sample B-0S) exhibits much weaker absorption due to OH deformation (Fig. 6). The high frequency OH band is particularly weakened and is shifted from 840 to 800 cm^{-1}. The 640 cm^{-1} band is broadened and difficult to distinguish from the adjacent feature at 690 cm^{-1}. ISHIKAWA and INOUYE (1975) found that as Cl was partially removed from the structural tunnels of synthetic β-FeOOH by exhaustive washing, the OH deformation bands diminished in intensity and shifted to lower frequencies. They speculated that the intensity reductions were due to the transformation of OH^- to O^{2-} to maintain electrical neutrality as Cl^- was replaced by H_2O.

Although the relative intensity of the 1040 cm^{-1} band in sample Bt-4 (also La-1 and Nb-1) may be enhanced due to trace amounts of jarosite, it is apparent from Fig. 6 that the IR spectra of both the natural and synthetic mine drainage samples are similar to that of poorly crystallized β-FeOOH with superimposed Fe-SO_4 absorption features. Of particular interest is the band at 610 cm^{-1} that can be attributed to $\nu_4(SO_4)$ (NAKAMOTO, 1986). This band is absent in the sulfated sample of B-0S and may provide a means of distinguishing structural and adsorbed SO_4 in samples of this type. Furthermore, the appearance of this band is associated with a decrease in the OH deformation at 640 cm^{-1} observed in akaganéite, indicating that SO_4 has displaced OH during formation of the mine drainage mineral. In contrast, the broad absorption feature in the 800–900 cm^{-1} region of most samples indicates residual OH in the structure as would be required to explain the full low temperature (100–400°C) weight loss observed with TGA (Fig. 5). Relative to sample B-0S, the Fe-O stretch band at 410–460 cm^{-1} is asymmetric in the mine drainage samples and may be influenced by $\nu_2(SO_4)$.

An assignment for the 690 cm^{-1} absorption feature remains problematic for both the mine drainage mineral and akaganéite. LAZAROFF (1983) attributed this band to $\nu_t(H_2O)$ in his bacterial precipitates, whereas KELLER (1970) assigned it to δ(OH) in akaganéite. The position and intensity of absorption is rather insensitive to tunnel composition (Cl, F) and to deuteration (KELLER, 1970); therefore, assignment to Fe-O stretch is perhaps more appropriate even though the band occurs at a higher frequency than similar vibrations in other iron oxyhydroxides. The absorption feature occurring at 1400 cm^{-1} in sample Y3b (also Y1 and La-1) is a COO-band arising from organic impurities and is weakened when the samples are treated with H_2O_2.

Mössbauer Spectra

Room-temperature Mössbauer spectra from sediment samples Bt-4 and Y3b and from synthetic sample Z500a (see

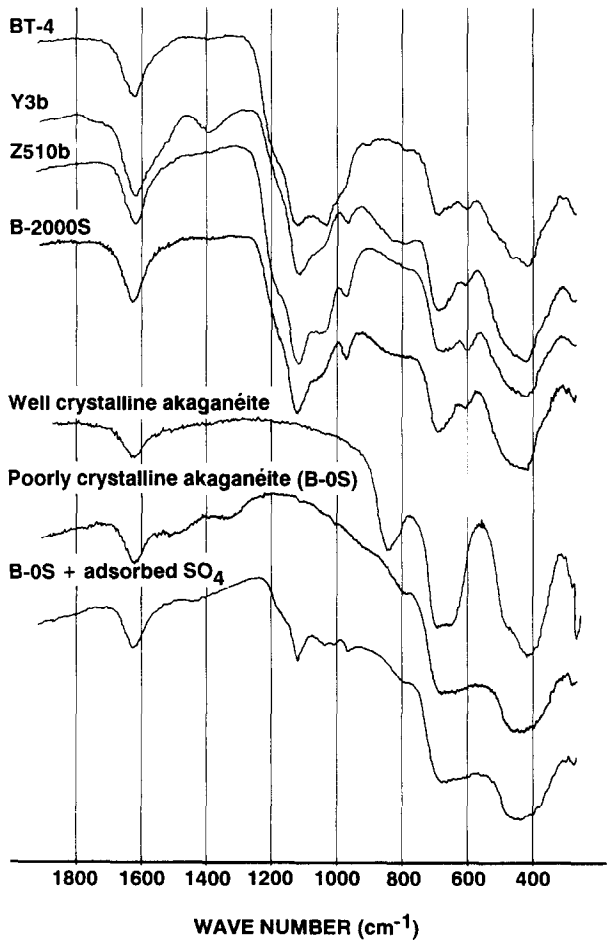

FIG. 6. Infrared spectra of selected natural and synthetic specimens. Sample B-0S analyzed both before and after SO_4 adsorption.

Table 7. Summary of infrared data for the mine drainage mineral and β-FeOOH

Mine Drainage Mineral		β-FeOOH	
	$- cm^{-1} -$		$- cm^{-1} -$
νOH	3300 - 3500[1,2]	νOH	3150 - 3350[3]
H_2O deformation	1620 - 1650[1,2]	H_2O deformation	1630[3]
$\nu_3 SO_4$	1170 - 1180 sh[2] 1110 - 1140[1,2] 1040 - 1070[2]		
$\nu_1 SO_4$	970 - 980[1,2]		
δOH	1045[1]		
δOH	800 - 880[2]	δOH	800 - 840[2,4,5]
$\nu_R H_2O$	670 - 700[3]		
Fe-O stretch (?)	670 - 700[2]	Fe-O stretch (?)	690[2]
		δOH	680[5]
		δOH	620 - 650[2,4,5]
$\nu_4 SO_4$	610 - 620[2]		
Fe-O stretch	410 - 460[2]	Fe-O stretch	410 - 460[2]
$\nu_2 SO_4$ (?)	420 - 440[2]		

1. Lazaroff et al., 1982.
2. This paper.
3. Lazaroff, 1983.
4. Ishikawa and Inonye, 1975.
5. Keller, 1970.

MURAD, 1988) consist of a broadened Fe(III) doublet. The low-velocity line in all cases has a higher dip and is narrower than the high-velocity line (Fig. 7). Spectra taken in an extended velocity range of ±10 mm/s show that this asymmetry is neither due to the presence of Fe(II) nor a result of relaxation due to incipient magnetic order. Because of their asymmetry, these spectra could not be properly fitted with distributions of quadrupole splittings having identical isomer shifts, a model that has proven suitable to fit the room-temperature spectra of most poorly crystalline iron oxides. Adequate results were obtained when the spectra were fitted with quadrupole-splitting distributions that assume a linear correlation between the quadrupole splitting and the isomer shifts or with two discrete quadrupole-splitting distributions that have different isomer shifts (Table 8). The former model assumes the isomer shift to vary linearly as a function of the quadrupole splitting, so that different incremental increases of the isomer shift with the quadrupole splitting parallel different extents of spectral asymmetry. The second approach implies the existence of two *discrete* iron sites within the structure of the mineral.

Independent of the fitting model, average quadrupole splittings of maximum probability for the natural and synthetic samples were about 0.65 mm/sec. This value is similar to that of relatively "well"-crystallized, 6 XRD-line ferrihydrite. Although the existence of quadrupole-splitting distributions rather than well-defined quadrupole splittings indicates significant variations of Fe-site symmetry, the distribution half-widths of the samples studied here (0.46–0.51 mm/sec for single distribution fits) are considerably narrower than those of even the best-crystallized ferrihydrites (about 0.72 mm/sec; MURAD et al., 1988), indicating less variation of Fe-site distortion than in the latter.

Mössbauer spectra of sample Z500a show the onset of magnetic order to be somewhat diffuse, with an average ordering temperature of about 75 K (Fig. 7). The application of a magnetic field of 6 T at this temperature or above did not induce magnetic order, suggesting that distributions of Néel temperatures rather than superparamagnetic relaxation are responsible for the gradual magnetic ordering. Fitting the magnetic components with a hyperfine field distribution showed the magnetic fields of maximum probability to increase from 38.4 T at 50 K to 45.4 T at 4.2 K. These fits also indicate the quadrupole interaction to have a considerably higher average value (−0.20 mm/sec) than in magnetically ordered ferrihydrite (−0.02 to −0.10 mm/sec).

Spectra of the magnetically ordered specimens taken at 4.2 K were clearly asymmetric, with a low-velocity line that has a higher dip but a narrower width than the corresponding high-velocity line. Distributions of hyperfine fields with identical isomer shifts and quadrupole interactions for all components, which give acceptable fits for the Mössbauer spectra of most poorly crystallized iron oxides at 4.2 K, could not be used to describe these asymmetric spectra. Better results were obtained using fits that imply variations of quadrupole splitting as a function of the hyperfine field or two discrete hyperfine field distributions with different isomer shifts and quadrupole splittings (Table 9). It is interesting to note that the latter is in contrast to akaganéite, the Mössbauer spectra of which can be fitted with three subspectra that have essen-

tially identical isomer shifts (MURAD, 1979). Regardless of the fitting procedure, the hyperfine fields of maximum probability are also lower than those of even the most poorly crystallized (2 XRD-line) ferrihydrites (MURAD et al., 1988) by about 1 T. Both the low ordering temperature and the low hyperfine field strongly indicate that some structural component, presumably SO_4, inhibits magnetic ordering in the mine precipitates.

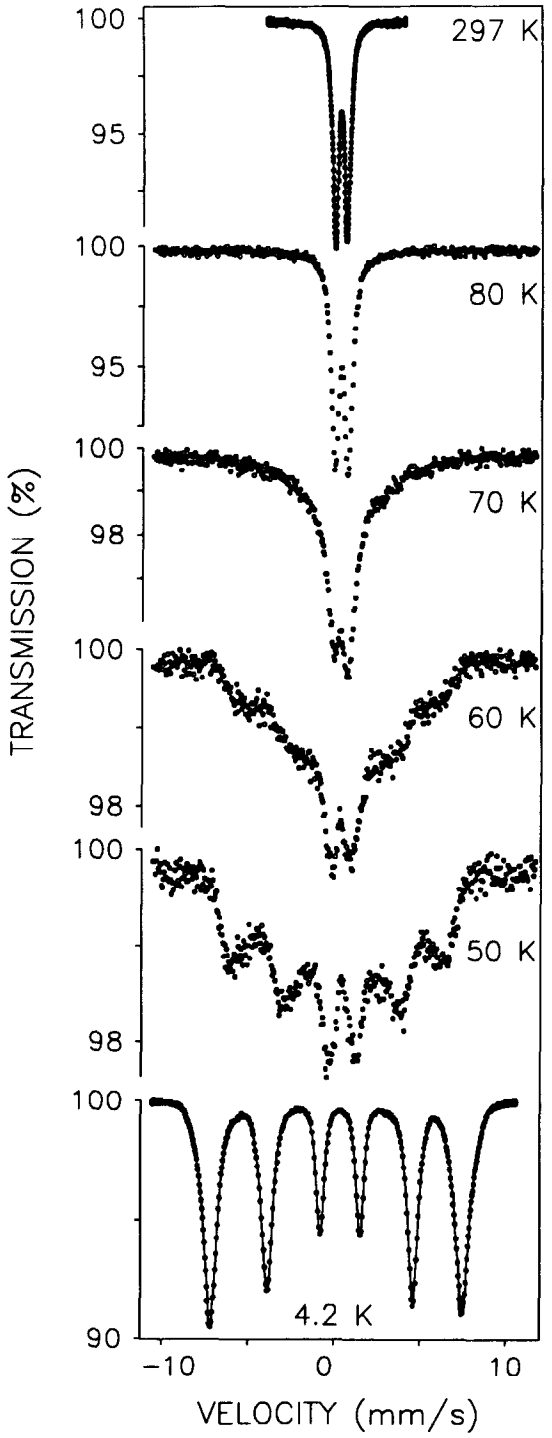

FIG. 7. Mössbauer spectra of synthetic precipitate Z500a at 297 and 4.2 K and in the vicinity of the Néel temperature.

Dissolution Kinetics and SO_4 Extraction

Dissolution-time curves for samples Bt-4 (Fig. 8) and La-1 (not shown) yield a plateau after 12 h indicating complete dissolution of the oxide fraction in 0.1 M HCl. The S-shaped portion of the curves produced from data collected at shorter time intervals presumably reflects a change in particle morphology (dissolution cavities, break up of aggregates, etc.) as the samples dissolve (SCHWERTMANN, 1984). By extrapolation of the curves to t_0, it is apparent that approximately 15% of the total SO_4 is immediately released, as compared to only 3 to 4% of the total Fe. This initial "burst" of SO_4 is probably derived from surface sites. Half-reaction times (t_{50}) for the remaining Fe and SO_4 are similar (Bt-4: $t_{50(Fe)} \simeq t_{50(SO_4)} \simeq 3.0$ h; La-1: $t_{50(Fe)} \simeq 6.0$ h, $t_{50(SO_4)} \simeq 5.4$ h), indicating congruent dissolution and dispersion of both species within the mineral structure. Differences in bulk dissolution rates between the two samples probably reflect differences in morphology. Sample La-1 consists of "grassy" spheres like those shown in Fig. 1e, whereas specimen Bt-4 is composed of a much looser aggregation of fibers.

While dissolution kinetics confirm that SO_4 occupies sites both on the surface and within the structure of the mine drainage mineral, they do not demonstrate conclusively that it is an *essential* structural component. If O bridging occurs between SO_4 and Fe at internal sites, extraction of the sulfate should destabilize the structure. To test this hypothesis, subsamples of natural specimen Bt-4 were equilibrated at room temperature in aqueous 0.05 M $Ba(NO_3)_2$ solutions (pH 3.0 to 3.5) for varying time periods. After 6 h, 35% of the SO_4 present in the acid soluble fraction (5.5 wt% SO_4) was extracted to form $BaSO_4$ without degrading the mineral structure. The amount extracted did not change significantly after 24 h, suggesting "equilibrium" with a defined fraction of "labile" SO_4. Even after 18 days, no detectable alteration of the 8-line diffraction profile was observed, indicating that most of the readily extractable SO_4 was derived from surface or near-surface sites. With prolonged equilibration for 77 days, additional SO_4 was extracted through a reaction that was presumably diffusion-controlled, and the sample was completely converted to goethite. This transformation supports an essential structural role for the remaining SO_4.

Proposed Structure

Poor crystallinity and small particle size prohibit a direct structural analysis of the mine drainage mineral or its synthetic analogs using XRD techniques, but data presented in this paper strongly support a structure similar to that of akaganéite. Akaganéite has a tetragonal unit cell with $a_0 = 1.054$ and $c_0 = 0.303$ nm (MURAD, 1979) and is composed of double chains of $FeO_3(OH)_3$ octahedra that share corners to yield square tunnels of 0.5×0.5 nm^2 extending parallel to the c axis. Each tunnel is composed of adjoining cavities formed by eight OH groups, and there is one cavity per unit cell. It has been estimated that these cavities can accommodate ions or molecules of up to 0.35 nm in diameter and that the necks

Table 8. Room-temperature Mössbauer parameters of synthetic bacterial and natural iron oxide precipitates from acid drainage environments.

Sample	Fit	Q_{max}	W_{dis}	δ/Fe	$\delta(\delta)$
Z500a	VARISO	0.63(1)	0.51	0.3491(4)	0.0040(1)
Y3b	VARISO	0.64(1)	0.46	0.348 (1)	0.0036(3)
Bt-4	VARISO	0.65(1)	0.46	0.3469(7)	0.0035(2)
Z500a	TWOISO	0.62(1) 0.62(1)	0.48 0.41	0.390 (2) 0.322 (3)	
Bt-4	TWOISO	0.68(1) 0.68(1)	0.37 0.37	0.391 (3) 0.328 (4)	

VARISO fits variable isomer shifts which increase from δ/Fe by $\delta(\delta)$ mm/s per 0.20 mm/s increment in quadrupole splitting; TWOISO fits two distributions of quadrupole splittings with discretely different isomer shifts. Q_{max} is the quadrupole splitting of maximum probability and W_{dis} the distribution half-width.

of the cavities are 0.27 nm in diameter (CHILDS et al., 1980). The diameter of Cl^- is approximately 0.36 nm. By comparison, the SO_4 ion is 0.50 nm in diameter and could not be accommodated in such cavities without sharing O with the surrounding Fe atoms.

It can reasonably be assumed that hydroxyls lining the faces rather than O comprising the corners of each tunnel would be responsible for such bridging. Distances between the centers of exposed hydroxyls on the same, adjacent, and opposite faces of a cavity are approximately 0.30, 0.35, and 0.50 nm, respectively (Fig. 9a), compared with an O-O distance in the free SO_4^{2-} ion of 0.26 nm (PARFITT and SMART, 1977). Bonding between SO_4 and adjacent Fe atoms on the *same* face would involve the least distortion of the bidentate complex but would require the remaining S (0.06 nm) and two O (each 0.26 nm in diameter) of the SO_4 ion to occupy a single cavity in the tunnel, which is not possible. Bonding to Fe atoms on two adjacent sides of a cavity to form a bridged bidentate complex of type -Fe-O-SO_2-O-Fe- would permit the remaining S and the two "free" O in the SO_4 ion to occupy two adjacent cavities parallel to the tunnel axis (Fig. 9b). Such bonding could not be achieved without distortion of the structure, but distortion is consistent with the poor crystallinity of the mineral.

Additional evidence to support this bonding mechanism can be derived from the IR and Mössbauer results. NAKAMOTO (1986) suggests that it is possible to distinguish between bidentate and bridged bidentate complexes, both with C_{2v} symmetry, on the basis that the highest SO frequency of the bidentate groups normally lies above 1200 cm^{-1} while the bidentate bridging complexes yield frequencies below 1200 cm^{-1} as observed with the mine precipitates. The formation of bidentate bridging complexes would require that two distinctly different Fe sites occur in the structure, one in which Fe sits in its usual octahedral coordination with O and OH as $FeO_3(OH)_3$ and one in which OH is replaced by SO_4 to yield $FeO_3(OH)_2O$-SO_3. Based on the proposed structural model (Fig. 9b), the ratio of these sites should be 1:3. The physical existence of two such sites is supported by Mössbauer spectroscopy data (Tables 8 and 9) which can readily be interpreted to indicate two distributions of quadrupole splittings in the paramagnetic state and two distributions of magnetic hyperfine fields with different quadrupole interactions in the magnetically ordered state; however, the area ratio of the subspectra is approximately 1:1.5. The discrepancy between predicted and experimental results may reflect the difficulty of determining accurate area ratios due to a distribution of parameters caused by short-range variations in structure that

Table 9. Mössbauer parameters at 4.2K of synthetic bacterial and natural iron oxide precipitates from acid drainage environments.

Sample	Fit	B_{max}	W_{dis}	δ/Fe	Q	δ(Q)
Z500a	VAREQ	45.4(1)	4.4	0.493(1)	-0.399(4)	0.023(1)
Y3b	VAREQ	45.6(1)	4.5	0.488(1)	-0.375(8)	0.020(1)
Bt-4	VAREQ	45.0(1)	4.9	0.488(1)	-0.363(5)	0.019(1)
Z500a	TWODIS	45.2(1) 45.6(1)	3.9 3.9	0.489(1) 0.501(1)	-0.362(3) 0.001(3)	
Bt-4	TWODIS	44.9(1) 45.0(1)	4.6 4.6	0.493(1) 0.477(2)	-0.329(4) -0.027(6)	

VAREQ fits variable quadrupole interactions which increase from the minimum Q by δ(Q) mm/s per 1.5 T increment in hyperfine field; TWODIS fits two distributions of hyperfine fields with different quadrupole splittings and isomer shifts. B_{max} is the hyperfine field of maximum probability and W_{dis} the distribution half-width.

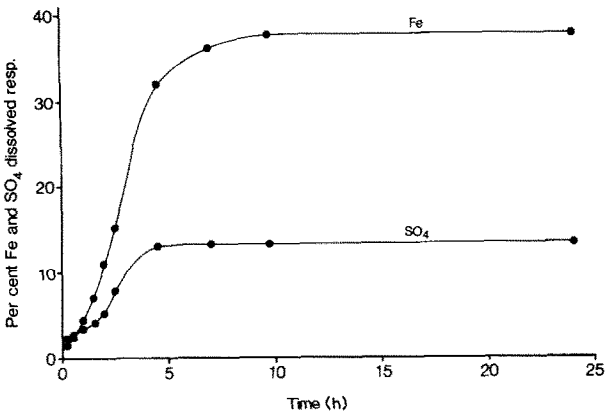

FIG. 8. Release of Fe and SO_4 from sample Bt-4 as a function of time by dissolution in 0.1 M HCl.

may include incomplete saturation of the tunnel sites with SO_4 (see following discussion).

Because the "free" O of the structural SO_4 must occupy two tunnel cavities, a doubling of c_0 relative to akaganéite (a_0 = 1.054 nm, c_0 = 0.303 nm, space group = I/4 m) would be required to accommodate the SO_4, as shown in Fig. 9b. Average unit cell lengths derived from XRD analyses of the natural specimens (Bt-4, La-1, Nb-1, and Y3b) would then be a_0 = 1.065 and c_0 = 0.604 nm (Table 6). Experimentally, a doubling of c_0 and an assignment of space group P4/m is supported by XRD data for the proposed (200, 111) peak centered at approximately 0.5 nm (Table 6). Analyses of 22 natural and synthetic specimens show an apparent migration of this peak from the calculated position of d_{200} (0.533 nm) toward that of d_{111} (0.471 nm) with increasing SO_4 content (Fig. 10). Diffraction from (111) is prohibited with space group I4/m but is not restricted with space group P4/m. Since d_{200} should actually occur at a slightly *higher* spacing (relative to akaganéite) with the proposed value of a_0, we must assume that the observed peak "migration" actually reflects increased diffraction from d_{111} relative to d_{200} with increasing SO_4 content and that the broad character of the peaks prohibits the resolution of a diffraction doublet. A direct comparison of line indices using both the akaganéite and the proposed (enlarged) unit cell is provided in Table 6.

In the proposed structure, a unit cell includes 16 Fe octahedra surrounding 2 cavities of the central tunnel. In addition, the contents of 4 adjacent tunnels are shared with adjoining unit cells. If all tunnel sites are filled, the unit cell formula would be $Fe_{16}O_{16}(OH)_{12}(SO_4)_2$, with an Fe/S ratio of 8.0. This ratio is consistent with that observed for sample Y1, but approximately 25% of the tunnel sites in this specimen must be occupied by Cl (Table 5). Furthermore, a ratio of 8.0 is substantially greater than those obtained from the other specimens. In particular, samples Bt-4, La-1, and Nb-1, with an average Fe/S ratio of 5.0, would conform more closely to a formula of $Fe_{16}O_{16}(OH)_{10}(SO_4)_3$. If the proposed structural model is accurate, these stoichiometric discrepancies can only be explained by adsorption of significant quantities of SO_4 on the particle surfaces as indicated by dissolution, Ba-extraction, and IR data.

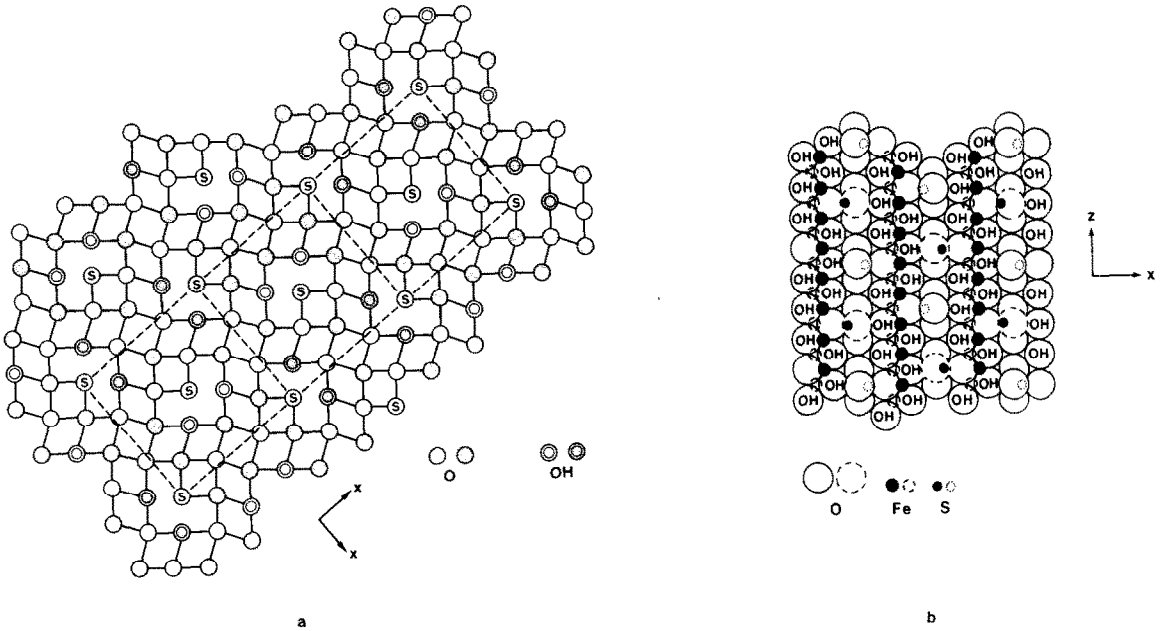

FIG. 9. Proposed structural model of the mine drainage mineral (a) perpendicular to "z" with open and shaded circles indicating oxygens or hydroxyls occurring in and below the plane of the paper, respectively. Circles labelled "s" denote tunnel oxygens comprising part of the SO_4 ion; (b) parallel to "z" with solid and broken lines indicating atoms occurring in and below the plane of the paper, respectively. Both drawings are shown without distortion.

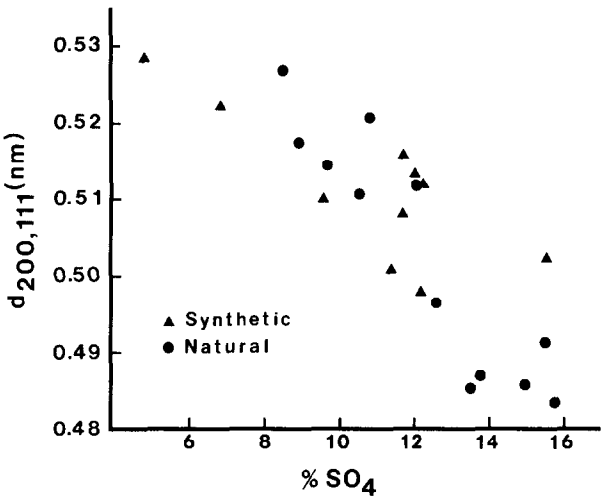

FIG. 10. Relationship between $d_{200,111}$ and SO_4 content for 22 natural and synthetic specimens.

In samples such as Y1 and Y3b, the tunnel positions are presumably filled with both Cl and SO_4, and any excess SO_4 is specifically adsorbed at surface sites. Other specimens such as Bt-4 and Nb-1, that are formed from very sulfatic solutions (Table 2) and that contain little Cl, should be near saturation with respect to SO_4 in both surface and tunnel positions. Assuming that SO_4 exchanges only with singly coordinated (A-type) hydroxyl groups on the surface to form a bidentate bridged complex (PARFITT and SMART, 1978), it is possible to calculate a theoretical adsorption maximum for an oxide with an akaganéite-type structure displaying primarily (100) and (010) faces. Each face should contain two A-type hydroxyl groups within an area of 0.637 nm^2, thereby yielding a maximum adsorption capacity of 2.6 μmol SO_4 m^{-2}. A specimen with 250 m^2/g surface area could thus accommodate a maximum of 6.2 wt% adsorbed SO_4. When the total chemical data (Table 5) are adjusted to reduce the SO_4 contents by an amount corresponding to maximum adsorption, samples Bt-4 and Nb-1 yield Fe/S mole ratios of 7.9 and 7.8, respectively. The calculated adsorption maximum for sample Bt-4 (5.6 wt%) also corresponds well with that obtained experimentally by Ba extraction (5.5 wt%). All other specimens yield higher ratios since they are apparently not at saturation with respect to SO_4.

Most of the analyses presented in Table 5 also include more structural H_2O [$H_2O_{(800)}$] than would be permitted by the proposed unit cell formulation(s). SCHWERTMANN et al. (1985) observed that goethites of varying crystallinity retained a monolayer of chemisorbed water after heating to 80°C. If such water is included in the $H_2O_{(800)}$ measurements, the total chemical data can be further refined by estimating the amount of adsorbed water in monolayer coverage from the measured surface areas and assuming a cross-sectional area for a H_2O molecule of 0.108 nm^2. The resulting calculations (Table 10) are in reasonably good agreement with the proposed formulae having Fe/S ratios ranging between 8.0 and 5.3. Calculated mineral densities corresponding to these ratios would be 3.75 and 3.90 g/cm^3, respectively.

Measurements from electron micrographs (e.g., Fig. 1d) show that the acicular structures protruding from surfaces of the particles are approximately 30 nm (or 3 unit cells) in width. The needles are also very thin, indicating preferential growth parallel to the needle axis which is, presumably, in the *c* direction. Thinness perpendicular to *c* is consistent with disappearance of the 110 XRD line with increasing SO_4 (Fig. 4), since the development of this reflection would require extended order in the *a* and *b* dimensions of the crystal. In contrast, the 004 reflection at 0.15 nm reflects the full length of the needles and is usually the sharpest diffraction line (Table 6). Figure 9a shows the approximate cross-sectional area of a needle and also serves to illustrate the unit cell and proposed SO_4 bonding perpendicular to *c*.

CONCLUSIONS

We believe the mineral described in this paper is the principal compound formed by bacterial oxidation of Fe(II) in acid sulfate ecosystems (e.g., acid mine effluents; acid sulfate soils) within the pH range 2.5–4.0. It has not previously been identified due to poor crystallinity and has commonly been referred to in the technical literature as "amorphous ferric hydroxide" or sometimes mistakenly as ferrihydrite. It is distinguished from ferrihydrite by a tunnel structure similar to

Table 10. Total chemical analyses adjusted for CO_2 and adsorbed H_2O.

Sample	Fe_2O_3	SO_3	As_2O_5	Cl	H_2O
	----------	----------	----------	%----------	----------
Bt-4	77.7	16.2	0.7	0.5	6.3
La-1	80.3	15.1	-	1.3	5.1
Nb-1	76.6	15.3	-	0.2	8.8
Y1	83.2	10.1	1.6	2.3	2.5
Y3b	82.0	12.2	2.6	1.6	2.8
$Fe_{16}O_{16}(OH)_{12}(SO_4)_2$	82.7	10.3	-	-	7.0
$Fe_{16}O_{16}(OH)_{10}(SO_4)_3$	79.5	14.9	-	-	5.6

that of akaganéite and from akaganéite by a SO_4 content averaging 12 to 16% by weight, yielding an Fe/S ratio in the range of 5.3 to 8. The latter represents a significantly higher ratio than can be attributed to often associated sulfate minerals such as jarosite. The tunnel SO_4 also creates distortion and subtle but distinct changes in structure relative to akaganéite.

The identification of this previously undefined compound can perhaps account for the anomolous mineral stability relationships reported from previous geochemical analyses of acid mine solutions (CHAPMAN et al., 1983; FILIPEK et al., 1987; KARATHANASIS et al., 1988; SULLIVAN et al., 1988) and strongly suggests that "amorphous iron oxide" may, in fact, embrace a variety of minerals. The clear role of SO_4 as a structural element also raises anew the issue of adsorption vs. precipitation reactions and their relative significance in reactions yielding or involving poorly crystallized Fe compounds.

Acknowledgments—The authors gratefully acknowledge the analytical skills provided by Ms. B. Gallitscher, Ms. C. Gutbord, Ms. G. Pfab, Mr. H. Fechter, and Mr. R. Winland. The latter also provided assistance in the collection of field samples. Dr. H.-Ch. Bartscherer prepared the TEM photos, and Mrs. E. Schuhbauer carefully drafted the figures. Prof. J. Torrent (Universidad de Córdoba) kindly provided the color measurements reported in Tables 3 and 4. Professors F. E. Wagner (T. U., München) and J. D. Cashion (Monash University) are thanked for allowing some of the low-temperature Mössbauer spectra to be taken on their spectrometers, and Prof. L. H. Bowen (North Carolina State University) is thanked for taking Mössbauer spectra between 50 and 80 K. Many helpful comments and ideas concerning interpretation of the XRD data were provided by Profs. P. Keller and K. M. Towe. Much of the laboratory work was conducted while the senior author was on sabbatical leave at the Institut für Bodenkunde in Freising-Weihenstephan, Germany. Financial assistance from the Alexander von Humboldt Stiftung and The Ohio State University during this period are deeply appreciated.

Editorial handling: R. G. Burns

REFERENCES

BRADY K. S., BIGHAM J. M., JAYNES W. F., and LOGAN T. J. (1986) Influence of sulfate on Fe-oxide formation: Comparisons with a stream receiving acid mine drainage. *Clays Clay Mineral.* **34,** 266–274.

CARLSON L. and SCHWERTMANN U. (1981) Natural ferrihydrites in surface deposits from Finland and their association with silica. *Geochim. Cosmochim. Acta* **45,** 421–429.

CARTER D. L., HEILMAN M. D., and GONZALES C. L. (1965) The ethylene glycol monoethyl ether (EGME) technique for determining soil-surface area. *Soil Sci.* **100,** 409–413.

CHAPMAN B. M., JONES D. R., and JUNG R. F. (1983) Processes controlling metal ion attenuation in acid mine drainage streams. *Geochim. Cosmochim. Acta* **47,** 1957–1973.

CHILDS C. W., GOODMAN B. A., PATERSON E., and WOODHAMS F. W. D. (1980) The nature of iron in akaganéite (β-FeOOH). *Australian J. Chem.* **33,** 15–26.

CROSBY S. A., GLASSON D. R., CUTTLER A. H., BUTLER I., TURNER D. R., WHITFIELD M., and MILLWARD G. E. (1983) Surface areas and porosities of Fe(III)- and Fe(II)-derived oxyhydroxides. *Environ. Sci. Tech.* **17,** 709–713.

ELLIS J., GIOVANOLI R., and STUMM W. (1976) Anion exchange properties of β-FeOOH. *Chimia* **30,** 194–197.

FARZANEH A. and TROLL G. (1978) Pyrohydrolysis for the rapid determination of chlorine traces in silicate and non-silicate minerals and rocks. *Fresenius Z. Anal. Chem.* **292,** 293–295.

FENCHEL T. and BLACKBURN T. H. (1979) *Bacteria and Mineral Cycling.* Academic Press.

FERRIS F. G., TAZAKI K., and FYFE W. S. (1989) Iron oxides in acid mine drainage environments and their association with bacteria. *Chem. Geol.* **74,** 321–330.

FILIPEK L. H., NORDSTROM D. K., and FICKLIN W. H. (1987) Interaction of acid mine drainage with waters and sediments of West Squaw Creek in the West Shasta Mining District, California. *Environ. Sci. Tech.* **21,** 388–396.

HARRISON J. B. and BERKHEISER V. E. (1982) Anion interactions with freshly prepared hydrous iron oxides. *Clays Clay Mineral.* **30,** 97–102.

ISHIKAWA T. and INOUYE K. (1975) Role of chlorine in β-FeOOH on its thermal change and reactivity to sulfur dioxide. *Bull. Chem. Soc. Japan* **48,** 1580–1584.

JACOBSEN J. (1976) Mobilization, transportation and sedimentation of weathering products from the abandoned brown-coal pits. (Iron pollution of the river Skjerna and Ringkobing fjord, Western Jutland). In *Geological Survey of Denmark, Yearbook 1975, Copenhagen,* pp. 57–74.

JANIK L. M. and RAUPACH M. (1977) An iterative, least-squares program to separate infrared absorption spectra into their component bands. *CSIRO Div. Soils Tech. Paper* **35,** 1–37.

KARATHANASIS A. D., EVANGELOU V. P., and THOMPSON Y. L. (1988) Aluminum and iron equilibria in soil solutions and surface waters of acid mine watersheds. *J. Environ. Qual.* **17,** 534–543.

KARLSSON S., SANDEN P., and ALLARD B. (1987) Environmental impacts of an old mine tailings deposit—metal adsorption by particulate matter. *Nordic Hydrol.* **18,** 313–324.

KELLER P. (1970) Eigenschaften von $(Cl,F,OH)_{<2}Fe_8(O,OH)_{16}$ und Akaganéit. *N. Jb. Mineral. Abh.* **113,** 29–49.

KLEINMANN R. L. P., CRERAR D. A., and PACELLI R. R. (1981) Biogeochemistry of acid mine drainage and a method to control acid formation. *Min. Eng.* **33,** 300–306.

LAZAROFF N. (1983) The exclusion of D_2O from the hydration sphere of $FeSO_4 \cdot 7H_2O$ oxidized by *Thiobacillus ferrooxidans. Science* **222,** 1331–1334.

LAZAROFF N., SIGAL W., and WASSERMAN A. (1982) Iron oxidation and precipitation of ferric hydroxysulfates by resting *Thiobacillus ferrooxidans* cells. *Appl. Environ. Microbiol.* **43,** 924–938.

LAZAROFF N., MELANSON L., LEWIS E., SANTORO N., and PUESCHEL C. (1985) Scanning electron microscopy and infrared spectroscopy of iron sediments formed by *Thiobacillus ferrooxidans. Geomicrobiol. J.* **4,** 231–268.

MACKENZIE R. C. (1957) The oxides of iron, aluminium and manganese. In *The Differential Thermal Investigation of Clays* (ed. R. C. MACKENZIE) Chap. 12, pp. 299–328. Mineral. Soc. London.

MARGULIS E. V., SAVCHENKO L. A., SHOKAREV M. M., BEISEKEEVA L. I., and VERSHININA F. I. (1975) The amorphous basic sulphate $2Fe_2O_3 \cdot SO_3 \cdot mH_2O$. *Russian J. Inorg. Chem.* **20,** 1045–1048.

MARSHALL N. J. (1978) Colorimetric determination of arsenic in geochemical samples. *J. Geochim. Expl.* **10,** 307–313.

MCKNIGHT D. M., KIMBALL B. A., and BENCALA K. E. (1988) Iron photoreduction and oxidation in an acidic mountain stream. *Science* **240,** 637–639.

MURAD E. (1979) Mössbauer and X-ray data on β-FeOOH (akaganéite). *Clay Mineral.* **14,** 273–283.

MURAD E. (1988) The Mössbauer spectrum of "well"-crystallized ferrihydrite. *J. Magnetism Magnetic Mater.* **74,** 153–157.

MURAD E., BOWEN L. H., LONG G. J., and QUIN T. G. (1988) The influence of crystallinity on magnetic ordering in natural ferrihydrites. *Clay Mineral.* **23,** 161–173.

NAKAMOTO K. (1986) *Infrared and Raman Spectra of Inorganic and Coordination Compounds,* 4th ed. J. Wiley & Sons.

NORDSTROM D. K. (1982) Aqueous pyrite oxidation and the consequent formation of secondary iron minerals. In *Acid Sulfate Weathering* (eds. J. A. KITTRICK et al.), Chap. 3, pp. 37–56. Soil Sci. Soc. Amer.

PARFITT R. L. and SMART R. ST. C. (1977) Infrared spectra from

binuclear bridging complexes of sulphate adsorbed on goethite (α-FeOOH). *J. Chem. Soc. Faraday I.* **73,** 796–802.

PARFITT R. L. and SMART R. ST. C. (1978) The mechanism of sulfate adsorption on iron oxides. *Soil Sci. Soc. Amer. J.* **42,** 48–50.

PATERSON E., SWAFFIELD R., and CLARK D. R. (1982) Thermal decomposition of synthetic akaganeite (β-FeOOH). *Thermochimica Acta* **54,** 201–211.

POWERS D. A., ROSSMAN G. R., SCHUGAR H. J., and GRAY H. B. (1975) Magnetic behavior and infrared spectra of jarosite, basic iron sulfate and their chromate analogs. *J. Solid State Chem.* **13,** 1–13.

SCHWERTMANN U. (1964) Differenzierung der Eisenoxide des Bodens durch photochemische Extraktion mit saurer Ammoniumoxalat-Lösung. *Z. Pflanzenernähr. Bodenkd.* **105,** 194–202.

SCHWERTMANN U. (1984) The influence of aluminum on iron oxides: IX. Dissolution of Al-goethites in 6 M HCl. *Clay Mineral.* **19,** 9–19.

SCHWERTMANN U. and FISCHER W. R. (1973) Natural "amorphous" ferric hydroxide. *Geoderma* **10,** 237–247.

SCHWERTMANN U., CAMBIER P., and MURAD E. (1985) Properties of goethites of varying crystallinity. *Clays Clay Mineral.* **33,** 369–378.

STUMM W. and MORGAN J. J. (1981) *Aquatic Chemistry,* 2nd edn. J. Wiley & Sons.

SULLIVAN P. J., YELTON J. L., and REDDY K. J. (1988) Solubility relationships of aluminum and iron minerals associated with acid mine drainage. *Environ. Geol. Water Sci.* **11,** 283–287.

TORRENT J. and SCHWERTMANN U. (1987) Influence of hematite on the color of red beds. *J. Sediment. Petrol.* **57,** 682–686.

TOWE K. M. (1981) Structural distinction between ferritin and iron-dextran (Imferon). *J. Biol. Chem.* **256,** 9377–9378.

TOWE K. M. and BRADLEY W. F. (1967) Mineralogical constitution of colloidal "hydrous ferric oxides." *J. Colloid. Interface Sci.* **24,** 384–392.

WINLAND R. L. (1989) Acid coal mine drainage in Ohio: Stream water quality, precipitate chemistry and mineralogy. M. S. thesis, The Ohio State University.